ELSEVIER

Journal of Molecular Catalysis A: Chemical 162 (2000) 443–462

JOURNAL OF MOLECULAR CATALYSIS A: CHEMICAL

www.elsevier.com/locate/molcata

Bulk and surface structure and composition of V–Sb mixed-oxide catalysts for the ammoxidation of propane

H.W. Zanthoff [a,*], W. Grünert [a], S. Buchholz [a,1], M. Heber [a,2], L. Stievano [a,b], F.E. Wagner [a,c], G.U. Wolf [a,d]

[a] *Lehrstuhl für Technische Chemie, Ruhr-Universität Bochum, D-44780 Bochum, Germany*
[b] *Institut de Recherches Sur la Catalyse, Avenue Albert Einstein 2, 69626 Villeurbanne Cedex, France*
[c] *Physik-Department E15, Technische Universität München, D-85748 Garching, Germany*
[d] *Institut für Angewandte Chemie, Berlin-Adlershof e.V., Richard Willstätter-Str. 12, D-12489 Berlin, Germany*

Dedicated to Professor Helmut Knözinger on the occasion of his 65th birthday.

Abstract

Vanadium–antimony mixed oxides, which are active and selective catalysts for the ammoxidation of propane to acrylonitrile, were obtained via different preparation routes and studied with a number of bulk and surface-sensitive techniques to elucidate the bulk composition of these complex materials and the character of their exposed surfaces. The V–Sb oxides were prepared via a redox reaction between NH_4VO_3 and Sb_2O_3 in an aqueous slurry, with subsequent calcination, or via a solid-state reaction between Sb_2O_3 and V_2O_5. The characterisation techniques employed were X-ray diffraction (XRD), N_2 physisorption, electron microscopy, potentiometric titration, Mössbauer, EPR, X-ray photoelectron spectroscopy (XPS), ion scattering spectroscopy (ISS), ultraviolet photoelectron spectroscopy (UPS), and IR spectroscopy. It was found that samples obtained by the solid-state reaction were more homogeneous than those prepared via the slurry route. The former consisted of (non-stoichiometric) $VSbO_4$ for $Sb/V = 1$, or a physical mixture of it with defective Sb_2O_4 for $Sb/V = 2$. Their bulk Sb/V ratio was found also for the surface region, the outmost part of which was enriched in vanadium to a small extent. Materials prepared via the slurry route consisted of (non-stoichiometric) $VSbO_4$, Sb_2O_4, and V_2O_5 if $Sb/V = 1$; the latter was missing for $Sb/V = 2$ and $Sb/V = 5$. While the character of the mixed surfaces was not determined by the V_2O_5 present, amorphous V oxide structures (highly dispersed species and aggregates) were supported on the Sb_2O_4 surface, which caused a significant vanadium excess in the overall surface composition in samples of $Sb/V > 1$. The average oxidation degree of the surface V species was higher than $4+$. Use of these catalysts in the propane ammoxidation reaction caused the surface V oxidation degree to approach $4+$ and diminished the degree of surface enrichment in vanadium. This was due both to a disappearance of the dispersed V entities and a decreased detectability of V oxide aggregates (aggregate growth or solid-state reaction with supporting Sb_2O_4). No evidence is available for surface spreading of Sb species as discussed in the literature.

Keywords: V–Sb mixed-oxide catalysts; Bulk structure; Surface structure; Ammoxidation of propane

* Corresponding author. Present address: Degussa-Hüls AG, Paul-Baumann-Str. 1, D-45764 Marl, Germany. Tel.: +49-234-32-28754; fax: +49-234-32-14115.

E-mail address: horst@techem.ruhr-uni-bochum.de (H.W. Zanthoff).

[1] Present address: Bayer AG, D-51368 Leverkusen, Germany.

[2] Present address: Institut für Oberflächen- und Mikrostrukturphysik, Technische Universität Dresden, D-01062 Dresden, Germany.

1381-1169/00/$ - see front matter
PII: S1381-1169(00)00337-X

1. Introduction

Vanadium–antimony mixed oxides are well known as active and selective catalysts for ammoxidation reactions of various hydrocarbons such as methylaromatics [1,2], propene [3] and propane [4,5]. During a mechanistic study of ammoxidation, it was found that these oxides also catalyse the selective reduction of NO to N_2, which is an undesired side reaction during ammoxidation [6]. Indeed, in a recent paper, Brazdil et al. demonstrated that the SCR-DeNO_x can be carried out on these solids between 673 and 733 K in a GHSV range of 3000–8000 h^{-1} [7].

For the ammoxidation of propane, it was observed that the catalytic performance of V–Sb oxide catalysts can be enhanced by addition of various promoter ions. Among these, tungsten, tin, and molybdenum gave highest selectivities and yields to the desired product acrylonitrile (ACN) (cf., e.g. [4,8–11]). These additives change the acidity as well as the redox properties of the V–Sb catalysts which dominate the catalytic performance [10].

The physicochemical bulk and surface properties of the $VSbO_4$ phase [12–14] and mixed V–Sb oxides [15–19] have already been investigated in the past. However, conflicting results were obtained by different characterisation methods and conflicting interpretations about the structure and composition were reported in the literature. This may be due to the fact that the structure of V–Sb mixed oxides strongly depends on the preparation method, which has been pointed out recently by Centi et al. [20].

Andersson and co-workers concluded from catalytic investigations combined with surface and bulk characterisation studies (e.g. [3,21–23]) that the only active phase in mixed V–Sb oxide catalysts is a non-stoichiometric $VSbO_4$ (labelled as '$\approx VSbO_4$'), in which surface enrichment in Sb creates isolated vanadium surface sites. This was suggested although XPS data indicated surface enrichment in vanadium for materials with $Sb/V > 1$ (volume ratios; samples prepared by a slurry technique, see below) [18]. This V enrichment was explained by the heterogeneity of the samples with varying sizes of crystallites of different surface composition. An increasing Sb/V surface ratio after use of the catalysts in propane ammoxidation was suggested to indicate that antimony spreads over the surface [18]. There are, however, conflicting reports about surface enrichment in V–Sb oxides. In other XPS work, Andersson et al. did not find clear indications for the surface enrichment of either V or Sb with slurry-prepared catalysts [16], and there was no surface enrichment in vanadium in slurry-prepared V–Sb–Sn oxides studied by Albonetti et al. [24]. Surface enrichment in antimony was reported for V–Sb oxides prepared by a solid-state reaction technique [25]. On the contrary, Centi et al. [26] suggested on the basis of Fourier-transform infrared spectroscopy in diffuse-reflectance mode (DRIFTS) work (lattice-vibration region, adsorption of NH_3 probe molecule) that the surface of $\approx VSbO_4$ is covered with an amorphous layer of V^{5+} oxide species. With increasing Sb/V ratio, the amount of this amorphous phase decreases, and the surface properties change from V-oxide to Sb-oxide characteristics. The supported V^{5+} species are reduced under reaction conditions, but still remain active. However, Centi et al. [26] also mention the presence of supported Sb oxide species.

This paper reports another attempt to elucidate the bulk and surface properties of V–Sb mixed-oxide phases of catalytic relevance. A multitechnique approach including a variety of methods capable of providing insight into the bulk and especially surface physicochemical properties has been applied. Techniques have been selected (XRD, N_2 physisorption, electron microscopy, potentiometric titration, EPR, Mössbauer spectroscopy, BET, XPS, ISS, UPS, DRIFTS[3]) that allow to examine mutual consistence of the results in order to derive a reliable picture of the structure and the surface composition of V–Sb oxides prepared via different routes (slurry and solid-state reaction).

2. Experimental

2.1. Catalyst preparation

Catalysts of the composition VSb_yO_x were prepared using two different methods adopted from the

[3] XRD — X-ray diffraction, XPS — X-ray photoelectron spectroscopy, UPS — ultraviolet photoelectron spectroscopy, ISS — ion scattering spectroscopy, DRIFTS — Fourier-transform infrared spectroscopy in diffuse-reflectance mode.

literature. Catalysts of compositions VSb_yO_x (y varying from 1 to 5) were prepared by an aqueous redox reaction between NH_4VO_3 (Fluka, > 99%) and Sb_2O_3 (Heraeus, > 99.99%), which was performed in a slurry (after [27]). The reaction mixture was stirred for 24 h under reflux. After removing the water under vacuum (353 K, 45 mbar), the residual was dried for 11 h at 413 K. Subsequently, the solid was intimately ground and calcined in air at 623 K for 24 h, at 773 K for 3 h and finally at 900 K for 3 h. Materials prepared via this slurry route will be denoted by their V/Sb ratio and the index (aq), e.g. VSb_1(aq) for VSb_1O_x obtained by the aqueous redox reaction. Alternatively, VSb_yO_x samples ($y = 1, 2$) were prepared by a solid-state reaction between Sb_2O_3 and V_2O_5 (Fluka, > 99.6%) (after [13]). These starting materials were intimately ground and calcined in air with a similar temperature programme as described above. The resulting V–Sb mixed oxides will be denoted by their V/Sb ratio and the index (s). α-Sb_2O_4 was prepared from Sb_2O_3 by calcination for 24 h in air at 1023 K.

The calcined samples were again intimately ground, pressed to pellets (2.5 t cm^{-2}, ca. 40 s), crushed and sieved. A fraction of $d_P = 255–350$ μm was used for the characterisation and catalytic experiments.

2.2. Physicochemical characterisation of catalysts

Bulk and surface physicochemical properties of the catalysts were determined before and after use in the ammoxidation of propane (see below) applying several methods.

2.2.1. Bulk characterisation

Bulk morphology, structural and redox properties were determined using XRD, TEM/EDX, potentiometric titration, Mössbauer-, EPR, and FTIR spectroscopy. All samples were studied in the as-received state without further pretreatment, and post-catalytic investigations were performed on samples transferred through the atmosphere.

XRD patterns were recorded in a 2Θ range of 10–70° using a Phillips powder diffractometer PW 1050/25 with Cu Kα radiation. *IR spectra* (400–4000 cm^{-1}) were taken from powdered samples mixed with KBr (1:10) using a Perkin-Elmer FTIR-Spectrometer 1720 X equipped with a DRIFTS cell. The *bulk vanadium oxidation state* of selected catalysts was determined using an Fe/Ce potentiometric titration method which has been described in detail earlier [10].

^{121}Sb *Mössbauer spectra* were measured with a source of ^{121m}Sn in a matrix of $CaSnO_3$. The source was kept at 4.2 K in a liquid helium bath cryostat, whereas the absorber was kept either at liquid He temperature or at ambient temperature (293 K). The Mössbauer spectrometer was operated with a sinusoidal velocity waveform. For γ-ray detection, an intrinsic Ge detector was used. The spectra were fitted with appropriate superposition of Lorentzian lines using the MOS-90 software [28]. For each component, the relative intensities and positions of the eight spectral lines produced by the $7/2 \rightarrow 5/2$ M1 transition of ^{121}Sb were calculated from the Clebsch–Gordon coefficients and the Hamiltonian of the pure quadrupole interaction, respectively. In this way, spectral parameters such as the isomer shift (IS), the electric quadrupole splitting (QS), the full line-width at half maximum (LW), and the relative resonance areas (Area) of the different components of the absorption patterns were determined. Fit results for spectra measured at 4.2 K are reported in Table 2. The IS's are referred to the $CaSnO_3$ source.

EPR investigations of the catalysts used in the present work have already been reported in detail elsewhere [29]. Their main conclusions will be included in the discussion.

2.2.2. Surface characterisation

Surface properties were investigated using nitrogen physisorption and XPS, UPS, ISS, and DRIFT spectroscopic techniques. BET surface areas were determined by N_2 physisorption at 77 K using a one-point method [30].

XPS, UPS, and ISS measurements were performed with a Leybold LHS 10/100 MCD spectrometer. The powdered samples were ground, and deposited onto a stainless-steel sample holder from a slurry of *n*-pentane. *XP spectra* were measured with Al Kα excitation (1486.6 eV, 12 kV × 20 mA) and recorded with constant pass energy (PE) of 35.5 eV. Since it is known from the literature that Sb(III) and

Sb(V) oxidation states have very close binding energies (chemical shifts of 0.3–0.8 eV are reported [31,32]), the XPS binding energy (BE) scale was referenced to Sb $3d_{3/2}$ = 540.0 eV. With this secondary reference, the C 1s signal of adventitious carbon was found at ≈ 284.7 eV. X-ray satellites were deconvoluted from the spectra with the software package 'Macfit' [33]. Atomic ratios were calculated from the Sb $3d_{3/2}$ and V $2p_{3/2}$ lines using the Scofield photoemission cross-sections [34].

UP spectra were measured using HeII excitation (40.82 eV), with an analyser PE of 23.7 eV. To avoid surface charging, the spectra had to be measured at elevated temperatures (for experimental details see [35], where minimum temperatures at which UP spectra were accessible have also been given). To allow comparison between samples, UP spectra of V–Sb mixed oxides reported in this paper were obtained at an identical sample temperature of 773 K. No change of the spectra was noted during data acquisition, which was complete in ≈ 15 min.[4] From the raw spectra, the HeIIb satellites were removed with the 'MacFit' software ([33], see also [35]).

Ion-scattering spectra were measured using 1000 eV He^+ ions (PE = 192 eV, scattering angle −135°). As for UPS, the charging problem was solved by keeping the samples at elevated temperatures during measurement. Forty scans with an emission current of 3 mA (sample current density ≈ 2.5 μA mm^{-2}) were performed on each sample. From the ion dose and the sputter yields at 1 keV primary energy, it was estimated that about four monolayers were erased during this series.

Surface acidic properties were determined by recording the DRIFT spectra of adsorbed pyridine. The powdered catalysts (10–20 mg) were first heated in the DRIFT cell to 773 K in a flow of N_2 to remove loosely bound species from the catalyst surface. Then, the catalysts were cooled down to room temperature and a pyridine/N_2 saturated gas stream (10 ml min^{-1}) was fed to them. The reversibly adsorbed pyridine was removed by flushing in N_2 for 0.5 h. Subsequently, DRIFT spectra were taken in the range of 400–4000 cm^{-1}.

[4] Due to the considerably longer acquisition times in XPS, which results in considerable risk of sample damage, measurement of XP spectra at elevated sample temperatures to minimise surface charging was not attempted.

2.3. Catalytic investigation

The catalytic properties of the slurry-prepared catalysts were tested in a micro-catalytic fixed-bed reactor under atmospheric pressure. Catalyst (3.6 g) was heated in N_2 to a reaction temperature of 793 K. A reaction mixture (100 ml min^{-1}) containing C_3H_8, O_2, NH_3, and He (1:1.6:2:5.4) was fed over the catalyst for 5–10 h. The product gas composition was determined by gas chromatographic analysis, which provided mass balances always better than 95%.

The catalysts prepared by solid-state reaction were only tested under non-stationary conditions. The pretreatment and reaction conditions to which they were subjected were close to those applied to the slurry-prepared samples.

3. Results and discussion

In the following, the bulk and surface physicochemical properties of the freshly prepared catalysts, and for selected samples, those after catalysis also, are described.

3.1. Bulk catalyst characterisation

3.1.1. XRD

The X-ray patterns (Fig. 1) reveal that the freshly prepared V–Sb–O catalysts consist of different crystalline phases depending on the composition and the preparation method. The slurry-prepared sample VSb_1(aq) exhibits not only the reflections of the expected ≈ $VSbO_4$ phase (rutile, JCPDS no. 35-1485 [36]), but also those of V_2O_5 (orthorhombic, JCPDS no. 9-387) and α-Sb_2O_4 (orthorhombic, JCPDS no. 11-0694). The exact composition of ≈ $VSbO_4$, and hence, lattice parameter and distribution of V oxidation states depend on the environment as mentioned in Section 1. The cation positions are filled with Sb^{5+}, V^{4+} and V^{3+} only; no Sb^{3+} or V^{5+} were

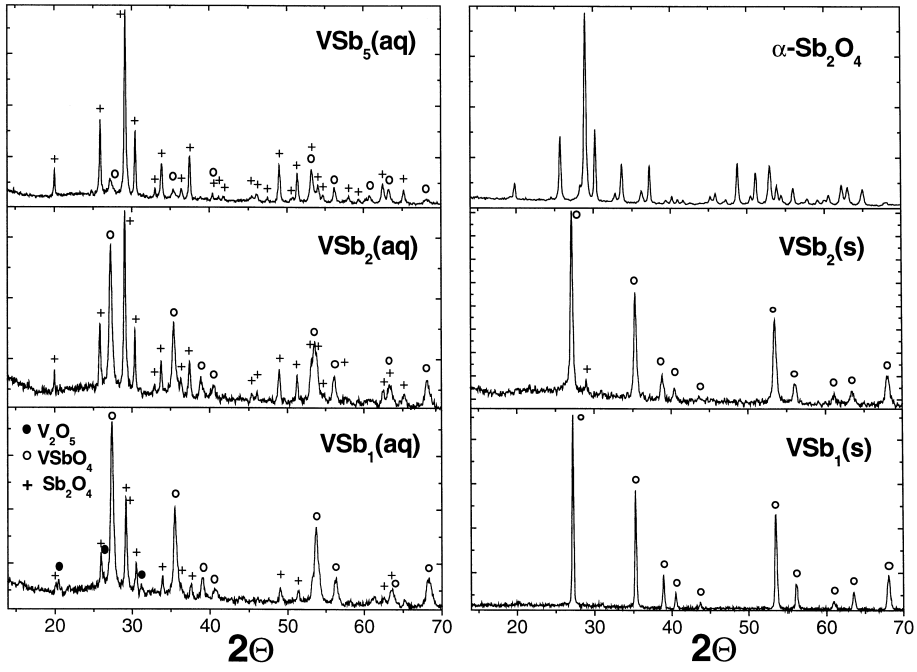

Fig. 1. XRD pattern of V–Sb oxide catalysts prepared (a) by the slurry method and (b) by the solid-state method and α-Sb_2O_4 as reference substance. Symbols: ● — V_2O_5; ○ — $VSbO_4$; + — Sb_2O_4.

detected in the pure ≈ $VSbO_4$ phase [15]. From Fig. 1, it can be seen that the intensities of α-Sb_2O_4 reflections increase with increasing Sb content (VSb_2(aq), VSb_5(aq)), while those of ≈ $VSbO_4$ decrease simultaneously. Crystalline V^{5+} phases could not be detected in these materials.

In the catalysts VSb_1(s) and VSb_2(s) prepared by solid-state reaction, the only crystalline phase detectable was ≈ $VSbO_4$ (cf. Fig. 1). In VSb_1(s), the crystallinity of the ≈ $VSbO_4$ phase was significantly higher than in the slurry-prepared catalysts as indicated by the smaller reflection half width, while the corresponding signals were broad and of low intensity in VSb_2(s). In the latter, crystalline Sb oxide phases were absent despite the excess of antimony. Reflections of other crystalline phases such as (VO)Sb_2O_4 [37] were not observed as well. The former may be explained by assuming that the transport phenomena occurring during the build-up of the most stable phase (here ≈ $VSbO_4$) will leave the initial material highly defective. The latter is due to the preparation conditions, which are far from the reductive conditions required for the formation of (VO)Sb_2O_4.

The pure antimony oxide Sb_2O_4 exhibited the reflections for α-Sb_2O_4 with small amounts of contamination by unconverted Sb_2O_3 (JCPDS no. 43-1071) (cf. Fig. 1).

3.1.2. FTIR spectroscopy, lattice vibrations

V–Sb mixed oxides exhibit characteristic absorption bands in the IR lattice-vibration region (1100–100 cm^{-1}) of which the range > 400 cm^{-1} was studied in the present work (cf. Fig. 2). The assignment of the observed absorption signals is, however, complex due to changing extinction coefficients, defect structures, different degree of crystallisation, heterogeneity of the catalysts, which results in severe overlap of the bands which in addition are mostly very broad. Therefore, different assignments have been proposed by research groups involved in the characterisation of V–Sb oxides. A compilation of data taken from the literature is given in Table 2.

3.1.2.1. Vanadium-rich samples, region below 750 cm^{-1}. The pure ≈ $VSbO_4$ phase has a rutile structure [13]. In general, the observable bands of mixed-

oxide rutile structures are very broad due to the possible fluctuations of local composition. However, characteristic wave-number ranges for different classes of vibrations have been determined as reported by Rocchiccioli et al. [38]: $\nu_1 = 730–630\ cm^{-1}$, $\nu_2 = 580–500\ cm^{-1}$, $\nu_3 = 380–250\ cm^{-1}$, $\nu_4 = 190–160\ cm^{-1}$ (cf. Fig. 2). The catalysts prepared in the present work exhibit vibrational bands at 650–680 and 530–560 cm^{-1} in accordance with the rutile structure of $\approx VSbO_4$. However, these bands cannot be identified in catalysts with low V content due to an overlap with the dominating vibrational bands of Sb_2O_4.

3.1.2.2. Antimony-rich samples. With increasing Sb content, bands at 746, 603 and 530 cm^{-1} become visible which can be attributed to ν_{Sb-O} vibrations of distorted octahedrally and tetrahedrally coordinated Sb in Sb_2O_4 [17,40] (cf. Fig. 2). Bands occurring at 1200 and 1107 cm^{-1} were assigned to Sb–O stretching vibrations close to defect centres by Centi and Mazzoli [40]. This explanation is supported by our data, since this band grows with increasing antimony content and does not change under reductive vacuum conditions (Fig. 3). Bands at 890 or 910 cm^{-1} [39,40] which were assigned by Centi et al. to an Sb^{5+} oxide species on the surface of

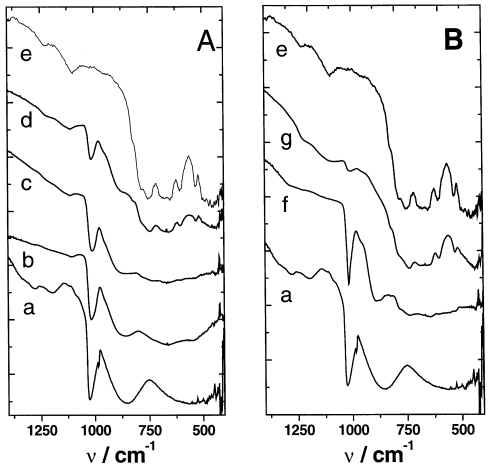

Fig. 2. DRIFT spectra of V–Sb mixed oxides and the corresponding binary oxides. A: (a) V_2O_5, (b) VSb_1(aq), (c) VSb_2(aq), (d) VSb_5(aq) and (e) Sb_2O_4. B: (a) V_2O_5, (f) VSb_1(s), (g) VSb_2(s), and (e) Sb_2O_4 (10 wt.% in KBr, respectively, measured in nitrogen atmosphere under ambient conditions).

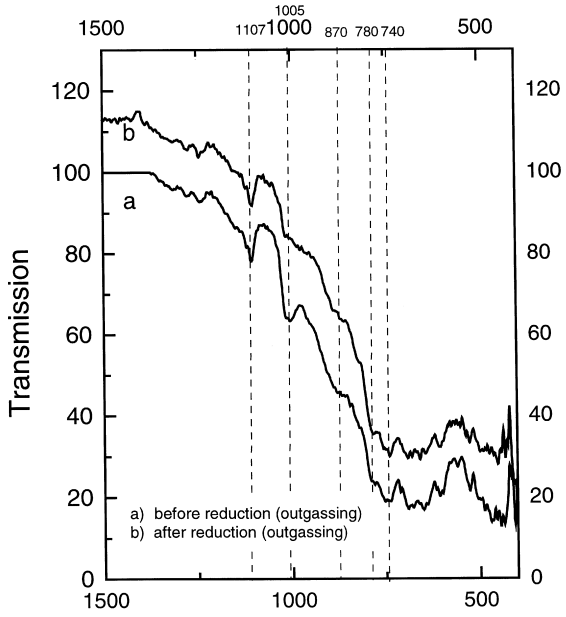

Fig. 3. The influence of a reductive treatment on the IR band at 1005 cm^{-1} — FTIR spectra of VSb_5(aq) before and after oxygen desorption (flowing He, 1073 K).

calcined $\approx VSbO_4$ samples and were reported to disappear during the ammoxidation reaction could not be observed in the present study. It will be shown below that our catalyst surfaces were enriched in V rather than in Sb.

3.1.2.3. Region between 750 and 1100 cm^{-1}. The bands observed at 1005–1016 and 850–860 cm^{-1} for all investigated catalysts cannot be assigned to the rutile structure [38]. Centi and Mazzoli [40] proposed these bands to belong to amorphous V^{5+} oxide species on top of $\approx VSbO_4$ (cf. Fig. 2). These bands decrease under reducing conditions (after thermally induced desorption of O_2 (cf. Fig. 3), and also in the presence of NH_3 or hydrocarbons [40,41], or upon calcination in N_2 [19]). Following the interpretation of Centi et al., the decrease is due to the reduction of the V^{5+} overlayer. On the other hand, Andersson et al. [19] suggested that these bands are not indicative for V^{5+} (or Sb^{5+}), but instead, arise from defect centres in $\approx VSbO_4$. This assignment was based on several observations: the 1010 cm^{-1} band also exists in Sb-rich samples with average V oxidation states below 4.00 (cf. Table 1, Fig. 2) and

Table 1
Average vanadium oxidation state of V_2O_5 and different V–Sb oxides as determined by potentiometric Ce/Fe titration

Catalyst	Average vanadium oxidation state	Calculated amounts of different oxidation states (%)	
		V^{4+} ($+V^{3+}$)[a]	V^{5+}
V_2O_5	4.92	8	92
VSb_1(aq)	4.35/4.04[b]	65	35
VSb_2(aq)	4.20/3.68[b]	80	20
VSb_5(aq)	3.81	100	–

[a] Assuming the oxidised form $Sb_{0.92}{}^{5+}V_{0.85}{}^{4+}\square_{0.23}O_4$.
[b] Centi et al. [17].

also in 'pure' $\approx VSbO_4$, in which only V^{4+} and V^{3+} sites were identified (see [19]). Moreover, it persists after ammoxidation [22]. These authors ascribed the decrease in the 1010 cm^{-1} band under reductive conditions to a simultaneous decrease in the number of defect sites [19]. A further explanation for the bands under discussion, which has not yet been proposed in the literature, would be the surface oxidation of the rutile phase resulting in the formation of terminal $V^{5+}=O$ sites, which would also be expected to decay under reductive conditions.

In this situation, the overtone vibrations of the observed signals may provide additional evidence in support of the correct interpretation. For V_2O_5, the overtones of the $V^{5+}=O$ vibrations have been reported to appear at 2020 and 1972 cm^{-1} [42,43] (as compared to 1020 and 980 cm^{-1} of the fundamental vibrations). Fig. 4 shows for the slurry-prepared VSb_x(aq) samples that these bands occur at the wave numbers typical of V_2O_5. For overtones of a rutile lattice vibration, a significant shift relative to the $V^{5+}=O$ overtones would be expected due to different degrees of anharmonicity. The position of the overtone bands supports, therefore, the presence of an amorphous V^{5+} oxide structure of the catalyst surface. On the other hand, it is known from the literature that two-dimensional $V^{5+}O_x$ layers which do not fully cover the carrier surface as present in the V_2O_5 (1 wt.%)–TiO_2 eurocatalyst [42] do not exhibit significant intensity at 1020 cm^{-1}. We assume, therefore, that the V^{5+} oxide species indicated by this band is segregated in amorphous or microcrystalline clusters. Indeed, it has been shown by isotopic reaction studies, which are reported elsewhere [44], that the catalysts expose different types of active vanadium structures.

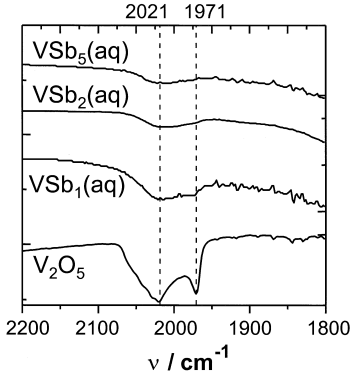

Fig. 4. DRIFT spectra of the overtone region of $V^{5+}=O$ stretching vibrations for (a) V_2O_5, (b) VSb_1(aq), (c) VSb_2(aq), and (d) VSb_5(aq).

3.1.3. Potentiometric titration

As mentioned above, vanadium in $\approx VSbO_4$ has the formal oxidation states V^{4+} and V^{3+} [17,19,45], their ratio depending on the oxygen partial pressure. The stoichiometry limits are represented by the formulae $Sb_{0.92}{}^{5+}V_{0.85}{}^{4+}\square_{0.23}O_4$ and $Sb_{0.9}{}^{5+}V_{0.2}{}^{4+}$-$V_{0.9}{}^{3+}O_4$ that have been reported for the oxidised and the reduced form, respectively [19]. Therefrom, the possible range for the average vanadium oxidation state can be calculated to vary from 4.00 to 3.18. The V oxidation states for the investigated samples are reported in Table 1. Values in excess of 4.00 as determined for VSb_yO_x ($y=1$, 2) (analogously reported by Centi et al. [17]) demonstrate that these samples contain additional V^{5+} which is not located in the rutile lattice and is largely X-ray amorphous according to the XRD and TEM/EDX (see below) results. With increasing Sb content, the average vanadium oxidation state of the catalysts

decreases which indicates a decreasing relative amount of amorphous V^{5+} sites.

3.1.4. Mössbauer spectroscopy

^{121}Sb Mössbauer spectra of VSb_2(aq) and VSb_5(aq) taken at 4.2 K are shown in Fig. 5. The spectra of all samples arise from two different spectral components (Table 2). The first, with a rather negative IS of $\approx -15\,mm\,s^{-1}$, is typical of Sb^{3+} in α-Sb_2O_4 [46]. The second component is typical of Sb^{5+}, having an IS of $\approx 0\,mm\,s^{-1}$. This component may represent α-Sb_2O_4 and $VSbO_4$. These two compounds, in fact, produce Sb^{5+} components with practically the same hyperfine parameters and cannot be resolved. Sb_6O_{13} also has similar IS's for Sb^{5+}, but its presence in significant amounts can be excluded by the observed shift of Sb^{3+} (Table 2).

The Sb^{3+} component is very weak in the spectrum of VSb_1(s), which contains virtually only Sb^{5+}. Combining this result with the observation that the material consists of only one phase — $VSbO_4$ (XRD, TEM/EDX, see below), it must be concluded that the $VSbO_4$ phase contains antimony only in the formal 5+ redox state, which is in accordance with earlier results of Berry et al. [14]. On the contrary, the other samples contain both Sb^{3+} and Sb^{5+} in significant amounts, with the Sb^{3+} content increasing monotonously with the overall Sb loading.

^{121}Sb Mössbauer spectra measured at room temperature show the presence of the same components (data not reported), but with a slight decrease in the relative intensity of the Sb^{3+} component. Since the measurements have been made sequentially with the same sample, source, and spectrometer, the change in the spectral intensities with temperature can be assumed to be directly proportional to that of the Lamb–Mössbauer *f*-factors, which can therefore be estimated. The quite similar value of the *f*-factors obtained for the Sb^{3+} and Sb^{5+} components at 4.2 K (not reported) allow the assumption that their relative resonance areas are directly proportional to the relative atomic content of Sb^{3+} and Sb^{5+}. Using this hypothesis and considering that all antimony exists either as $VSbO_4$ or as α-Sb_2O_4, and that vanadium other than in $VSbO_4$ exists only in the 5+ state, the relative amounts of these two species, and therefrom the distribution of the vanadium oxidation states, can be calculated. The results given in Table 2 show that the V^{5+} content is highest in VSb_1(aq), but decreases with increasing Sb content of the catalyst. VSb_5(aq) does not contain any significant amount of V^{5+}. These results are consistent with the V^{5+} amounts that were calculated form the average V oxidation states determined by potentiometric titration (cf. Table 1) under the assumption that vanadium in the 4+/3+ state exists only in the $VSbO_4$ phase.

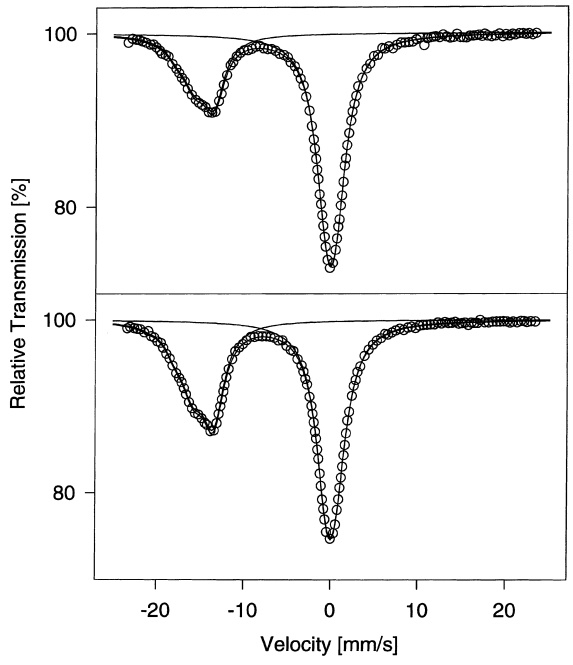

Fig. 5. ^{121}Sb Mössbauer spectra of freshly prepared VSb_2(aq) (top) and VSb_5(aq) (bottom) samples.

3.1.5. TEM / EDX

Electron microscopy of the investigated VSb_x(s) and VSb_x(aq) catalysts revealed the presence of $\approx$ $VSbO_4$ and α-Sb_2O_4 particles. Fig. 6 shows micrographs from VSb_2 samples prepared via the slurry route (right) and via solid-state reaction (left). Several different phases can be seen which have been identified by EDX, and in some cases, by electron diffraction. The image selected from the VSb_2(s) preparation shows both a $\approx VSbO_4$ and an Sb_2O_4 crystal. In addition, Sb oxide with O/Sb ratio ≈ 2 occurs in the sample in the form of small amorphous

Table 2
Oxidation states of antimony for the catalyst samples and pertinent reference materials obtained from Mössbauer spectra

Catalyst	^{121}Sb parameters at 4.2 K (mm s^{-1})			Sb redox state distribution (%)		Calculated phase composition (%)		Calculated vanadium composition (%)[a]	
	IS[b]	QS[b]	LW[b]	Sb^{3+}	Sb^{5+}	Sb_2O_4	$VSbO_4$	$(V^{3+} + V^{4+})$	V^{5+}
α-Sb_2O_4	−14.4[c]	16.4[c]	3.13[c]						
	(0.61)[c]	(−6.1)[c]	(3.31)[c]	0.91[c]	1[c]				
$Sb_2O_{4.35}$	−14.76[c]	17[c]	3.17[c]	0.42[c]	1[c]				
	(1.12)[c]	(−)[c]	(3.31)[c]						
Sb_2O_5	–	–	–						
	(1.06)[c]	(−4.3)[c]	(3.49)[c]	–	1[c]				
$V_{0.92}Sb_{0.92}O_4$	–	–	–						
	(−0.15)[d]	(n.d.)[d]	(3.52)[d]	–	1[d]	–	100		
VSb_1(s)	−15.3	16	3.0						
	(−0.26)	(4.1)	(3.70)	1	99	2	98	n.d.[e]	n.d.
VSb_1(aq)	−14.76	15.1	2.51						
	(−0.16)	(5.4)	(2.83)	15	85	30	70	64	35
VSb_2(aq)	−14.92	14.7	2.78						
	(−0.08)	(5.5)	(2.97)	30	70	60	40	74	26
VSb_5(aq)	−14.87	15.3	2.83						
	(0.02)	(5.5)	(3.02)	39	61	78	22	20	–

[a] Assuming the oxidised form $Sb_{0.92}V_{0.85}O_4$.
[b] Values for Sb^{3+}, and in parentheses, for Sb^{5+}.
[c] From [61], compositions given as compositional indexes.
[d] From [12], compositions given as compositional indexes.
[e] n.d.: not determined.

aggregates ($d < 10$ nm) as can be seen on the edges of the Sb_2O_4 crystal. Such a morphology of the Sb oxide phase, which is in fact much more abundant than the large crystals in our samples, has been

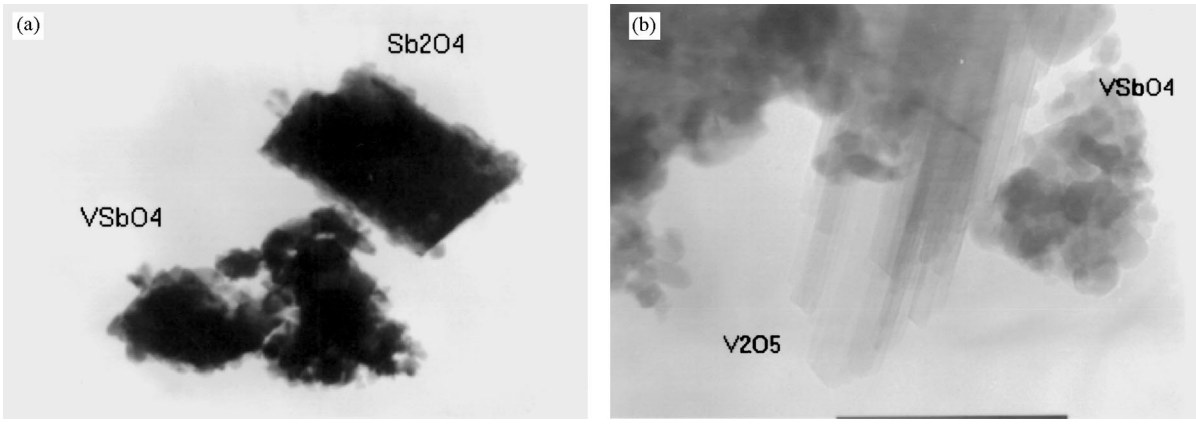

Fig. 6. TEM images of ≈ $VSbO_4$ and α-Sb_2O_4 particles in VSb_2(s), magnification — 20,000 (left), and of ≈ $VSbO_4$ and V_2O_5 particles in VSb_2(aq), magnification — 80,000 (right).

reported earlier in the literature [47]. The same phases are present in VSb_2(aq), but in addition, V_2O_5 could be detected, which exhibited a characteristic needle shape (cf. Fig. 6, right-hand side image). It should be noted, however, that V_2O_5 was present only in a minority of the particles, which explains that it escaped detection by XRD in VSb_2(aq). The selected micrograph shows nicely the morphology of $\approx VSbO_4$ forming aggregates of small crystallites largely surrounding the V_2O_5 crystals where these are present. In electron diffraction, the reflections from the small $\approx VSbO_4$ aggregates appeared as rings rather than as points.

3.2. Surface characterisation and catalysis

3.2.1. External surface area

BET surface areas of the investigated samples are reported in Table 3. All catalysts exhibit small surface areas typical for bulk mixed oxides ranging from 2 to $10\,m^2\,g^{-1}$. The mixed oxides possess larger areas than the pure oxides. The surface areas determined by the one-point method were somewhat different with different charges of samples (± 1–$3\,m^2\,g^{-1}$). Similar areas were reported in literature (cf. Table 3).

3.2.2. XPS and ISS

Table 4 summarises the results of the XPS and the ISS measurements with fresh V–Sb catalysts and with samples used in the catalytic reaction. The XP spectra are similar to those reported in the literature [18,48]; hence, only the V $2p_{3/2}$ signals are reproduced here (cf. Fig. 7a). Fig. 7b shows the IS spectrum (V and Sb signals) of a sample and its evolution with increasing acquisition time, i.e. upon sputtering of the surface.

In the as-prepared state, the V $2p_{3/2}$ BE of all V–Sb mixed oxides is between the ranges reported in the literature for V^{5+} in V_2O_5 (517.4–517.6 [49–51]) and V^{4+} in VO_2 or reduced V_2O_5 (516.1–516.4 eV [50–52]). Although the presence of other cations and the different character of the V–O bonds may exert some influence on the binding energies, this result is a strong indication that both V^{4+} and V^{5+} are present in the surface region. This can be clearly seen in the asymmetry of the V $2p_{3/2}$ signal of VSb_1(aq) and VSb_1(s) in Fig. 7a. Such asymmetry is not present in any of the Sb signals (not shown). The remaining samples exhibit a broader, more symmetric V line shape. Since this line-width increase is paralleled by a similar broadening of the Sb signals, it is difficult to decide as to which extent it is due to the coexistence of different V states or due to surface-charging effects. A quantitative analysis of V states was, therefore, not attempted.

In the as-prepared state, the Sb/V atomic ratios obtained by XPS exhibit characteristic trends (cf. Table 4). The data for the slurry-prepared materials are mostly within the ranges given by Andersson et al. [18,53], which are cited in parentheses. Remarkably, the VSb_1(aq) preparation exposes a surface, which has the same elemental composition as the overall sample. With increasing bulk Sb/V ratio, a significant surface enrichment in vanadium may be noted. On the other hand, the surface composition of the two catalysts obtained by the solid-state preparation is identical to their bulk composition irrespective of the bulk Sb/V ratio.

Table 4 reports also the evolution of the ISS Sb/V intensity ratio with increasing Sb content. It may be noted that the more surface-sensitive ion-scattering spectroscopy confirms the observation from XPS that the increase in the bulk Sb/V ratio is more clearly reflected in the surface of samples prepared via the solid-state route. Since atomic concentrations are not easily evaluated from IS spectra, Table 4 reports the trend of the Sb/V intensity ratio, with the value of VSb_1 ((aq) or (s)) set to 1. For the solid-state preparation, the increase in the bulk Sb/V ratio leads to the expected change in the Sb/V ISS intensity ratio, while the slurry preparation leads to

Table 3
BET surface area of the V–Sb–O samples prepared by solid-state reaction (s) and slurry reaction (aq)

Catalyst	S_{BET} / $m^2\,g^{-1}$
Sb_2O_4	2.2 (0.6)[a]
VSb_1(s)	2.0 (2)[a]
VSb_2(s)	3.8 (2–3.6)[a]
V_2O_5	2.0 (5.1–7.8)[a]
VSb_1(aq)	6.0–6.3 (10.6)[a]
VSb_2(aq)	4.1–9.5 (3.6)[a]
VSb_5(aq)	2.6–3.6 (1.4)[a]

[a] Taken from [20,21,62].

Table 4
Influence of composition and preparation method on the surface properties of V–Sb–O catalysts[a]

Sample	Bulk Sb/V	Before catalysis					After catalysis		
		BE(V $2p_{3/2}$)/eV	Sb/V (XPS)	Sb/V (XPS)[b]	Sb/V[c] (ISS)[c]	BE(V $2p_{3/2}$) (eV)	Sb/V (XPS)	Sb/V (XPS)[b]	Sb/V (ISS)[c]
Slurry preparation									
VSb_1(aq)	1	516.8	1.07 (0.7–1.2)[d]	1.10	1	516.3	1.03 (1.1)	0.93	1.2
VSb_2(aq)	2	516.8	1.46 (1.5)[d]	1.43	1.3	516.2	1.65 (2.7)	1.74	1.7
VSb_5(aq)	5	516.9	2.76 (1.8–12.6)[d]	3.20	2.8	516.6	3.70 (16.5)	3.70	3.7
Solid-state preparation									
VSb_1(s)	1	516.8	1.02	0.90	1	516.5	–[e]	–[e]	–[e]
VSb_2(s)	2	516.5	2.05	1.80	2.0	516.3	1.96	2.20	2.3

[a] V 2p binding and Sb/V ratios are from XPS and ISS. XPS binding energies are referenced to Sb $3d_{5/2}$ = 540.0 eV.
[b] After ISS, with about four monolayers removed.
[c] Area ratio, relative to freshly prepared material with Sb/V = 1.
[d] From Andersson et al. [18,53].
[e] Inaccurate due to contamination.

excess vanadium on the surface. In fact, the Sb/V intensity ratios increase to the same extent as the XPS Sb/V atomic ratios. This should not, however, be overstressed because the ISS data are normalised to the spectrum of a particular sample (VSb_1(aq) or VSb_1(s)) whose exact surface composition in the outmost layer (ISS sampling region) is actually unknown.

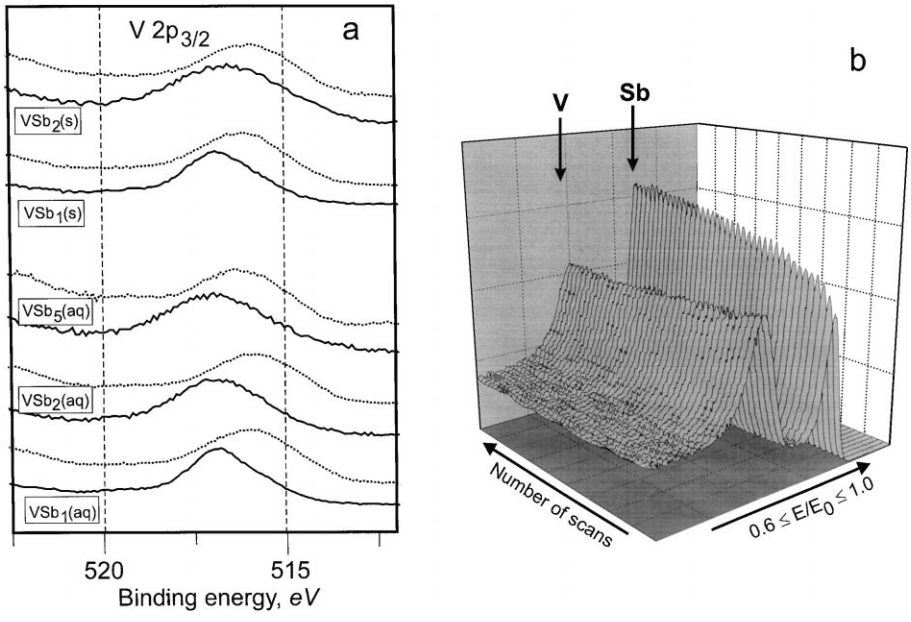

Fig. 7. XPS and ISS of V–Sb mixed oxides: (a) V $2p_{3/2}$ XP spectra of V–Sb catalysts in as-prepared form (solid lines) and after use in the ammoxidation of propane (dotted lines); (b) evolution of IS spectra with acquisition time (i.e. sputtering time), E_0 = 1000 eV.

Fig. 8 summarises the results of serial ISS scans (i.e. sputter series). In Fig. 8a, the evolution of the V and Sb signal intensities is given for one sample ($VSb_2(s)$) in its state prior to and after catalysis (upper part), and the resulting Sb/V ratios are plotted in the lower part. Fig. 8b reports the trends of these Sb/V ratios with increasing sputter time for the remaining samples. The data of $VSb_1(s)$ after catalysis are omitted since the data were compromised by an unidentified contamination in the outmost surface layer. It can be seen from Fig. 8 that the Sb/V ratio of the as-received samples generally increased with increasing sputter time. With $VSb_2(aq)$ and $VSb_5(aq)$, the rather steep initial increase is followed by a gradual further growth. With the remaining samples, in particular those prepared by solid-state reaction, the Sb/V ratio arrives at a constant level after 15–20 scans. From the post-catalytic measurements, it is quite obvious that Sb becomes more exposed by interaction with the reaction mixture. There is, however, no Sb enrichment in the external layers: the Sb/V ratio is almost constant during the sputter series, usually with slight increase in the first scans. Only in one case ($VSb_2(aq)$, Fig. 8b), there is a slight initial decrease in the Sb/V ratio, but this is not sufficient to establish a significant surface enrichment by Sb as would be expected from surface wetting by Sb species. Instead, the generally less pronounced increase in the Sb/V ratios after catalysis imply that part of the surface V species indicated by the trends with the as-received samples have been removed or clustered into larger aggregates.

Table 4 contains also the Sb/V atomic ratios measured by XPS after the ISS experiments. It appears that the surface composition of the samples that exhibit surface enrichment in V ($VSb_2(aq)$, VSb(aq) before and after catalysis) is not strongly affected by the removal of almost four atomic layers, despite the obvious change in the Sb/V intensity ratios in the ISS series (cf. Fig. 8). It should be noted that a quantitative relation between ISS and XPS cannot be established with our instrument since the XPS sampling area does not completely coincide with the area covered by ISS, but it has been shown that trends in ISS series are often reflected in strong intensity shifts in post-ISS analyses by XPS also in our experimental configuration (e.g. [54,55]). Thus,

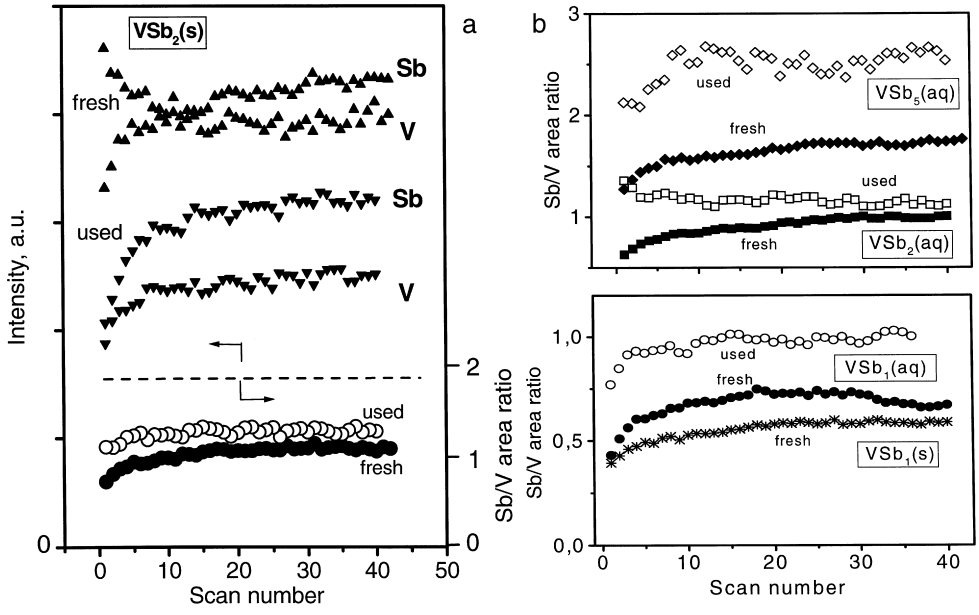

Fig. 8. Evolution of ISS Sb/V area ratios with increasing acquisition time (i.e. sputtering time): (a) development of V and Sb signal areas for $VSb_2(s)$ in as-prepared form and after use in the ammoxidation of propane, upper part — absolute signal areas, lower part — resulting Sb/V ratios; (b) development of Sb/V ratios for various Sb–V catalysts.

these data indicate that there are two vanadium enrichment layers: one is sputtered away to an appreciable extent by the removal of about four monolayers, while the other one is not significantly reduced during our experiment, where the ISS Sb/V ratios increase very slowly after ≈ 15 scans, although the surfaces are still enriched in V (e.g. VSb_2(aq), VSb_5(aq)). Hence, it may be concluded that the surface vanadium is present both as a very thin (probably monoatomic) layer and in the form of aggregates. It may be argued that the removal of a monoatomic surface layer of V should affect the XPS intensity measurements. On the other hand, considerations of photoelectron escape depths (estimate for V 2p — 1.67 nm [51]) lead to the conclusion that the contribution of this outmost surface layer to the total XPS signal intensity is limited to only 20–30%. Nevertheless, the lacking influence on the XPS intensities by the removal of the surface V species may imply that these cover only part of the surface exposed, and the particular strong effect observed with the Sb ISS signal (Fig. 8a) indicates that the vanadium is sputtered away from a pure Sb phase.

After the catalytic runs, the V $2p_{3/2}$ binding energies of all samples were significantly lower than in the as-received state (cf. Fig. 7, Table 4). Indeed, for several samples, the BE was well in the range typical of V^{4+} in oxide environment [50–52]. Obviously, the surface is more reduced than prior to the catalytic run, but the presence of oxidation states different from V^{4+} (in particular residual V^{5+}) cannot be ruled out due to the large line-widths and possible influences of the Sb environment on the binding energies of V oxidation states (vide supra). With VSb_2(aq) and VSb_5(aq), the surface enrichment in V has significantly decreased during the catalytic run. Again, this trend is also reflected in the ISS intensity ratios. These ratios became constant after 15–20 scans (cf. Fig. 8), although the vanadium enrichment traced by XPS was still significant with some samples after sputtering (VSb_2(aq) and VSb_5(aq) (Table 4)). Hence, the decreased surface enrichment in vanadium after catalysis, which is seen both by XPS and ISS, is rather due to the removal or clustering of vanadium species than to wetting by Sb. The vanadium species (dispersed and aggregated) may have formed clusters of larger sizes. More likely, some of them underwent solid-state reactions with the Sb_2O_4, resulting in the disappearance of some vanadium from the XPS and ISS sampling regions.

3.2.3. UPS

UPS has been recently successfully applied for the investigation of reduced surface states in V_2O_5 [51] and for the differentiation of binary and ternary oxide surfaces in Bi–Mo–O [35] and Ca–Ce–O mixed oxides [55]. The latter application is based on the observation that the O 2p valence band (VB) signals of oxides may form a suitable basis for fingerprint identification due to their characteristic shapes.

Fig. 9a shows UP spectra of the V–Sb mixed oxides and compares them with the spectra of V_2O_5 and Sb_2O_4. It may be noted that the VB of V_2O_5 has indeed a characteristic shape, which is discussed in more detail in [56], while the remaining materials exhibit just a broad asymmetric intensity maximum. There are some differences in the width and the position of this signal: with the materials prepared via solid-state reaction, its position shifts to higher BE and its width increases with the Sb content; hence, the shape of the VSb_2(s) spectrum is intermediate between those of VSb_1(s) and Sb_2O_4. The VB signals of the slurry-prepared samples do not shift and remain narrow even at high Sb content. To illustrate these relations, the signal maxima are marked and the VSb_1(aq) spectrum is repeated for comparison with each mixed-oxide spectrum in dotted lines.

At low BE (1.5–2 eV), another signal can be observed for the mixed oxides. This signal, which is known from reduced V_2O_5 [51], can be ascribed to the V 3d state of V^{4+} because the Sb 5s line appears at higher BE and is superimposed by the intense VB signal. UPS proves therefore the presence of reduced V states in the external surface layer(s) (average sampling depth ≈ 0.8 nm [51]), the concentration of which decreases with increasing Sb content of the samples. It should be noted that this does not imply an increasing average V oxidation state, because in UPS, the V^{4+} signal can be related only to an oxygen signal (O 2p). The oxygen is, however, coordinated to both V and Sb.

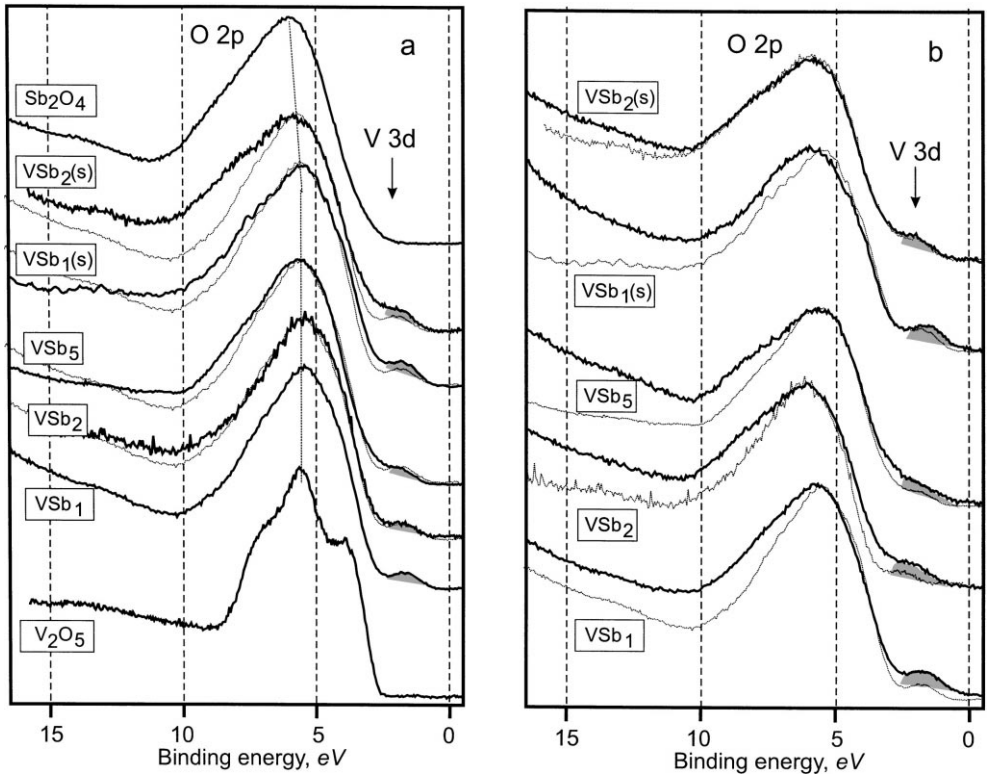

Fig. 9. UPS of V–Sb mixed oxides. (a) UP spectra of as-prepared V–Sb materials and binary oxides (V_2O_5 and Sb_2O_4), with the mixed-oxide spectra; the trace of VSb_1(aq) is repeated as dotted line for comparison. (b) UP spectra of samples after use in the ammoxidation of propane; shaded areas between 6.5 and 11 eV represent differences from spectra in as-received states.

After catalysis, the V^{4+} (3d) signal is more intense than in the as-received samples (Fig. 9a and b). The surface V species become more reduced by interaction with the reaction mixture as inferred already from the XPS results. By comparing spectra before and after catalysis, it was noted that, with some samples, the VB signal was significantly broadened after exposure to the reaction mixture. The corresponding differences have been shaded on the left-hand side of the VB signals in Fig. 9b. It should be noted that, for this comparison, the baselines had to be corrected to coincide at 0 and 13–15 eV. After these corrections, no significant changes could be noted for the remaining samples.

Analysis of the VB shapes shows that the surfaces of the slurry-prepared catalysts and of VSb_1(s) differ significantly from those of V_2O_5 and Sb_2O_4. Since there is no structure in the VB signal of any mixed oxide, it may be deduced that crystalline V_2O_5 is not exposed to an extent that determines the character of these surfaces. This is not in contradiction to the observation of V_2O_5 by XRD and electron microscopy in some of the samples (Figs. 1 and 6) since this phase occurred only in a minority of the particles and was partly covered by other material. However, it should be noted that the analysis of oxide structures by their UPS fingerprint is not capable of detecting minority species that may contribute to the overall surface in amounts of < 10–15%. For the materials prepared via solid-state reaction, the further interpretation takes advantage of results from XRD, electron microscopy, XPS, and ISS, according to which these materials are highly homogeneous in composition and elemental distribution (VSb_1(s): $\approx VSbO_4$, VSb_2(s): $\approx VSbO_4 + Sb$ oxides, mainly Sb_2O_4). We assume that the narrow VB signal exhibited by VSb_1(s) arises from $\approx VSbO_4$, while the broadening and shift observed for VSb_2(s) are due to

Sb oxides (mostly Sb_2O_4) coexisting with $\approx VSbO_4$. Hence, the surfaces of VSb_2(s) (and those of the slurry-prepared samples after catalysis) indeed expose the surfaces of physically mixed $\approx VSbO_4$ and Sb oxides (Sb_2O_4) as suggested also by the XPS and ISS results reported above. On the other hand, the surfaces of the fresh slurry-prepared samples are significantly different since the VB remains narrow even at high Sb content.

At the present level of experience with UPS on real oxide catalysts, it is, however, not possible to derive as to which type of surface species is responsible for the invariability of the VB shape in slurry-prepared V–Sb oxides (Fig. 9a). This invariability shows just that these surfaces do not expose the Sb_2O_4 detected by XRD to any significant extent, which is obviously due to the presence of V oxide species (thin overlayer, amorphous aggregates) detected by XPS and ISS. The VB signal of these entities must be, however, significantly different from that of V_2O_5; it should not exhibit a pronounced structure, resembling probably that of $\approx VSbO_4$ (cf. VSb_1(s) in Fig. 9a). A similar problem was encountered recently in a UPS study of V–Ti–O eurocatalysts [57]. While a contribution of V_2O_5 was easily discerned in the spectrum of EL10V8 (8 wt.% V_2O_5–TiO_2), the VB signal of EL10V1 (1 wt.% V_2O_5–TiO_2) did not differ significantly from that of the parent TiO_2, although XPS intensity measurements proved that vanadium was well dispersed over the TiO_2 surface. Due to the failure to discriminate between the VB signals of $\approx VSbO_4$ and the surface V species, no conclusion can be drawn about the impact of the catalytic run on the surface of VSb_1(aq).

3.2.4. DRIFT spectra of adsorbed pyridine

The surface acidity of V–Sb oxides has already been described in the literature on the basis of IR studies of ammonia adsorption [26]. However, since NH_3 reacts with the lattice oxygen of V–Sb oxides to N_2 and NO_x already slightly above room temperature [6], it is doubtful if NH_3 is a suitable probe molecule for the acidity of these surfaces. In our study, the acidity of VSb_y(ac) surfaces ($y = 1$, 2 and 5) was investigated with the pyridine probe ($pK_B \approx 5$). Pyridine is less basic than NH_3 ($pK_B \approx 9$) [58], but since it is also a relatively hard base [59], it gets adsorbed on the same acid sites as ammonia.

Fig. 10 shows IR spectra of pyridine adsorbed on the investigated V–Sb samples. The band positions together with the assignments proposed are summarised in Tables 5 and 6. In all spectra, the bands characteristic of pyridine adsorption on Lewis sites are found at 1580–1610 and 1440–1490 cm^{-1}. Bands at 1439, 1481 and 1582 cm^{-1} as found in all samples occur also in the spectrum taken with Sb_2O_4. They can obviously be assigned to Lewis sites on this surface, i.e. coordinatively unsaturated Sb ions. The bands increase with growing Sb content of the mixed oxides, and hence, Sb exposure. Bands at 1449, 1487, 1596 and 1605 cm^{-1} may be assigned to Lewis sites on V surface atoms (V_2O_5 [42], $\approx VSbO_4$). The shift of the band position to higher wave number shows that these sites are more acidic than those on Sb ions, but less acidic than those observed on an alumina surface, which have been included in Table 6 for comparison.

With the slurry-prepared samples, additional signals appear in the spectral region typical of pyridinium ions on Brønsted sites (≈ 1540 and $\approx 1638\,cm^{-1}$). Their wave numbers are also typical of vanadium-based sites (V–OH) [42]. These results

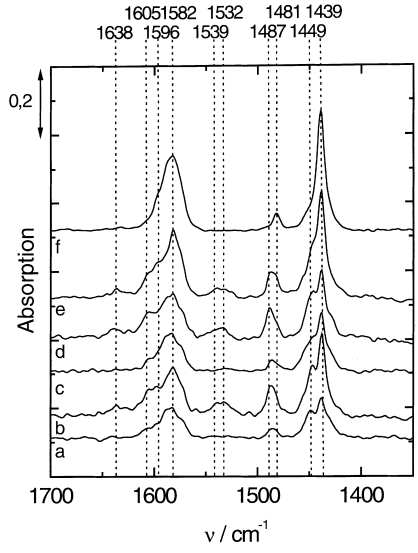

Fig. 10. DRIFT spectra of adsorbed pyridine on (a) VSb_1(s), (b) VSb_1(aq), (c) VSb_2(s), (d) VSb_2(aq), (e) VSb_5(aq), and (f) Sb_2O_4 (measured in nitrogen atmosphere under ambient conditions).

Table 5
IR lattice vibrations of antimony oxides, vanadium oxides and mixed V–Sb oxide catalysts and their interpretations in the literature

Experimental band position[a] / cm^{-1}	Assignment		
	Type of vibration	Position / cm^{-1}	Ref.
1005–1016 (vs)	ν^{b}_{Ome2} in $\approx VSbO_4$	1015–1020	[19]
	$\nu(V^{5+}=O)$ in V_2O_5	1020–1035	[42,63]
984 (w)	$\nu_{as}(V^{4+}-O)$	970–980	[63]
	$\nu(V^{5+}=O)^{c}$		[64,65]
810–850 (vb)	ν^{b}_{Ome2} in $\approx VSbO_4$	880	[19]
	$\nu_{as}(V^{5+}-O-V^{5+})$	820–830	[64]
$\approx$ 775 (vw)	ν_{Sb-O} in $Sb_2O_4^{d}$	770	[66]
746 (s)	ν_{Sb-O} in $Sb_2O_4^{d}$	745	[66]
635–700 (vb)	ν_{Sb-O} in $Sb_2O_4^{d}$	685	[66]
630–680 (vb)	ν_{Ome3} in $\approx VSbO_4$, rutile	630–670	[38]
603 (s)	ν_{Sb-O} in $Sb_2O_4^{d}$	610	[66]
530 (s)	ν_{Sb-O} in $Sb_2O_4^{d}$	530	[66]
520–560 (vb)	ν_{Ome3} in $\approx VSbO_4$, rutile	500–580	[19]

[a] vb — very broad, vs — very strong, s — strong, w — weak, vw — very weak.
[b] Twofold co-ordinated oxygen (with cation vacancy).
[c] In amorphous or two-dimensional structures.
[d] Distorted octahedral or tetrahedral Sb.

show that V–Sb oxides may exhibit both Lewis and Brønsted acidic sites. The Lewis sites are of low and medium strength, while slurry-prepared V–Sb catalysts may contain rather strong Brønsted sites also ($1638\,cm^{-1}$).

3.2.5. Propane ammoxidation

The catalytic properties observed with the V–Sb mixed oxides prepared in this study will be reported in detail elsewhere. Only the most relevant features will be cited here. It was found that the activity of the slurry-prepared catalysts decreased only slightly with increasing Sb content (propane conversion — 9.4, 10.1, and 8.4% for VSb_1(aq), VSb_2(aq) and VSb_5(aq), respectively). At the same time, the acrylonitrile selectivity increased markedly (10.1, 21.4, and 26.9%), and the propene selectivity decreased (43.2, 33.7 and 31.6%). It should be noted that the total amount of valuable products, i.e. propene + acrylonitrile, did not change strongly with increasing antimony content; the sum of selectivities increased from 53.3 to 57.5%, respectively. Similar results are known from the literature [21,23].

Comparison between catalysts prepared by slurry preparation or via solid-state reaction can be made

Table 6
IR bands for pyridine adsorbed on V–Sb oxides and Al_2O_3 and their assignment

V–Sb oxides, ν / cm^{-1}	Al_2O_3, ν / cm^{-1}	Correlations between wave numbers for adsorbed pyridine and type of acidic site for Al_2O_3 as reported in the literature
1638	1639	Brønsted site (PyH^+)
	1634	Brønsted site (PyO)
	1620–1624	Coordinatively bound to a Lewis acid site with large strength (PyL)
1605	1610–1615	Coordinatively bound to a Lewis acid site with low strength (PyL)
1596	1590–1595	Coordinatively bound to an octahedral Lewis site (PyL) and to a Brønsted site (PyH)
1582	1578	Coordinatively bound to a Lewis site (PyL)
1530–1540	1540–1550	Brønsted site (PyH)
1481–1487	1490	Brønsted sites and/or Lewis site (PyH^+ and PyL)
1439–1449	1445–1455	Coordinatively bound to Lewis site (PyL)

only on the basis of data from non-stationary reaction experiments [60]. The materials prepared via sold-state reaction were slightly less active but exhibited higher selectivity towards the desired products.

4. Properties of V–Sb mixed oxides as seen in a multitechnique approach

A comprehensive characterisation of VSb_xO_y catalysts prepared by solid-state and aqueous slurry reaction was performed in the present work aiming mainly at the identification of the structure and composition of the surface and the bulk phases. A variety of mutually verifying methods were used, some of them (ISS, UPS, DRIFTS with pyridine) being applied to this type of solid material for the first time.

The results reported and discussed above (including the earlier work of e.g. Centi et al., Berry et al. and Andersson et al.) reveal that the V–Sb oxide catalysts investigated in the present work differ in their surface and bulk composition, heterogeneity, crystallinity, acidity and redox properties in dependence mainly on the preparation method and the V/Sb ratio.

4.1. Antimony species in V–Sb oxide catalysts

The V–Sb oxide catalysts investigated in the present work are heterogeneous in nature. They contain crystalline and microcrystalline pure- and mixed-oxide phases, α-Sb_2O_4, non-stoichiometric cation deficient $\approx VSbO_4$. The catalyst samples prepared all contain cations of antimony in its formal oxidation states Sb^{5+} and Sb^{3+}. In accordance with earlier work on single-crystal $\approx VSbO_4$ [15], it was concluded from the results of various techniques used in the present work that $\approx VSbO_4$ contains Sb in the oxidation state Sb^{5+} only. Sb^{3+} is present in Sb_2O_4 only.

In contrast to results reported in the literature [3,21–23], none of the preparation techniques applied here resulted in surface antimony enrichment. Surface wetting by Sb under catalytic reaction conditions as proposed by Andersson et al. [18] could not be deduced from our ISS results. Furthermore, a combination of bulk (Mössbauer, potentiometric titration) and surface techniques (ISS, XPS) reveal that Sb predominantly exists in $VSbO_4$ and Sb_2O_4. There was no indication of a surface $Sb^{5+}O_x$ phase.

4.2. Vanadium species in V–Sb oxide catalysts and their role in the ammoxidation reaction

The V–Sb oxide catalysts contain vanadium in the non-stoichiometric cation-deficient $\approx VSbO_4$ structure. In vanadium-rich samples, few crystallites of V_2O_5 may be present as well. In accordance with earlier work on single-crystal $\approx VSbO_4$ [15], it was concluded from the results of various techniques used in the present work that $\approx VSbO_4$ contains vanadium in the oxidation states V^{3+} and V^{4+}. However, the average V oxidation states determined for our samples reveal that vanadium forms additionally an amorphous surface $V^{5+}O_x$ phase, in particular if the catalyst is prepared in the slurry phase. In accordance with this, the oxidation state of V in the surface region was found to be between $4+$ and $5+$.

The surface-analytical study shows that the surface of samples prepared via solid-state reaction has the same composition as the bulk, with only minor surface enrichment of vanadium. Slurry preparation leads to heterogeneous samples, in which the Sb_2O_4 component is largely covered by X-ray amorphous $V^{5+}O_x$ entities (thin overlayer and amorphous aggregates). This leads to overall surface enrichment in vanadium for the Sb-rich materials, while the coincidence of bulk and surface V/Sb ratio in VSb_1 is spurious. The overlayer is highly dispersed but not dense, because the ISS technique always revealed the presence of antimony on the surface. These results are supported by earlier suggestions of Centi et al. based on IR spectroscopic data [26]. During catalysis, the oxidation state of surface vanadium approaches $4+$, the thin overlayer of V species is decreased, and the aggregates grow or undergo solid-sate reaction with Sb_2O_4 to form $VSbO_4$, which leads to a higher surface exposure of antimony.

EPR results obtained earlier with the present samples [29] are consistent with this picture. Two types of signals were identified by EPR — isolated VO^{2+} ions, which are located in the same host phase in all samples, presumably the XRD-amorphous $V^{5+}O_x$

phase, and interacting V^{4+} sites (V^{4+} pairs in Sb-rich samples), which are supposed to be V^{4+} sites in the $VSbO_4$ phase. It was also found by EPR that the V^{4+} amount in the catalysts grows under ammoxidation conditions. In-situ experiments in the presence of propane and/or oxygen allowed to establish that V^{4+} is involved in the catalytic reaction cycle. In particular, it was found that the V^{4+}–V^{4+} interacting sites (or pairs) take part in the catalytic reaction, whereas isolated V^{4+} sites are not active [29].

4.3. Influence of the preparation method on the catalyst structure

Although the slurry preparation technique might be expected to result in a more homogeneous elemental distribution, the materials prepared by this method exhibit a more complex bulk and surface structure than the solid-state prepared samples. The latter were more homogeneous in composition: the Sb/V ratio of the surface region coincided with that of the bulk; only in the outmost surface layer(s) was a slight enrichment in V detected by ISS. $\approx VSbO_4$ was the only crystalline phase detected in materials prepared via solid-state reaction, with excess antimony at Sb/V = 2 present largely in X-ray amorphous oxide particles.

The slurry preparation leads to heterogeneous samples, which contain crystalline Sb_2O_4 and V_2O_5 even at Sb/V = 1. Surface analysis shows that V_2O_5, where present, is not the predominantly exposed phase, and that the Sb_2O_4 component is covered by amorphous vanadium entities (thin overlayer and amorphous aggregates) to a significant extent (see above). The supported V species are in the 5+ oxidation state, i.e. the surface is more oxidised than the bulk.

This can be explained by considering details of the slurry preparation procedure. In the slurry redox reaction, most of the starting V^{5+} is reduced and Sb^{3+} is oxidised. However, since antimony is not completely accessible from the aqueous phase, part of the V^{5+} remains unaffected. During water removal, a non-homogenous precipitation occurs. First, Sb_2O_4 and $VSbO_4$ (or their precursors) precipitate, while part of the V^{5+} remains in the solution on top of the precipitate, which is therefore of a dark blue colour. On further water removal, this part of vanadium is precipitated onto the surface of the solid formed previously. Calcination in oxidative medium is obviously not suited to homogenise this complex solid mixture.

4.4. Methodological considerations: the relation of surface and bulk techniques

It should be noted that evidence by XRD and electron microscopy about the heterogeneity of the slurry-prepared materials (in particular VSb_1) greatly facilitated the interpretation of our surface-analytical data. Generally, the surface spectroscopies are not well suited to differentiate between changes that occur parallel or perpendicular to the surface (e.g. clustering or diffusion into the bulk). Although the ISS sputter series, with subsequent XPS, provide a tool to discriminate in-plane and in-depth changes, the present authors would have hardly arrived at the conclusion that the coincidence of surface and bulk compositions is spurious for VSb_1 without the complementary evidence from XRD and electron microscopy. Hence, this study exemplifies once more that only the combination of a multitude of characterisation techniques may result in reliable information about the surface properties of materials relevant for catalysis. In particular, the present example teaches that the results of bulk techniques may be of high relevance for the correct interpretation of surface data.

5. Conclusions

Vanadium–antimony mixed oxides derived from different modes of preparation and having varying Sb/V ratios have been characterised by a variety of

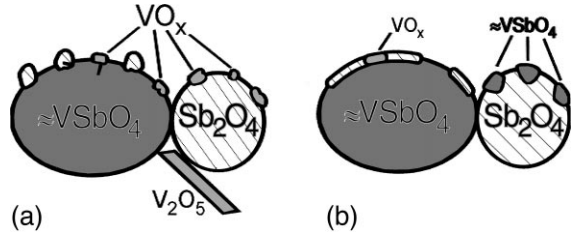

Fig. 11. Model of the structure and composition of V–Sb mixed oxides freshly prepared (a) and that of their surface and bulk transformations during ammoxidation of propane (b).

surface and bulk techniques (XRD, potentiometric titration, Mössbauer spectroscopy, XPS, ISS, UPS, DRIFTS, physisorption) to provide a consistent picture of their surface and bulk structure. The mixed oxides were prepared both via a redox reaction in aqueous medium followed by calcination (slurry preparation), and by a route involving only reaction in the solid state. It was found that the structure and the composition of V–Sb mixed oxides depend strongly on the preparation route, the conditions applied during calcination (e.g. atmosphere) and the overall Sb/V ratio. As described in the literature, the preparation techniques used in this work (slurry reduction, solid-state reaction) resulted in mixtures of several phases, which always contained $\approx VSbO_4$ (a rutile phase with cation defect sites), and also α-Sb_2O_4 and V_2O_5 depending on the Sb/V ratio. As suggested earlier by Centi et al. [26], the surface of these particles supports an amorphous V^{5+} oxide, the abundance of which depends on the preparation route and the Sb/V ratio. This V^{5+} oxide phase is present not only in the form of monolayer-dispersed species but also in the form of amorphous aggregates.

The surface structure of the catalysts changes during use in the propane ammoxidation, which is reflected in a decreased surface enrichment in V and a reduction of V sites. These changes indicate that solid-state reactions occur between the V and Sb components probably resulting in the formation of more $\approx VSbO_4$. Although this implies a mobility of Sb in the solid phase, a spreading of Sb species over the catalyst surface could not be observed.

A model of the catalyst structure deduced from the results of this study is given in Fig. 11.

Acknowledgements

Thanks are due to S. Wisniewski and A. Goman for performing BET and FTIR measurements.

References

[1] A.B. Azimov, V.P. Vislovskii, E.A. Mamedov, R.G. Rizaev, J. Catal. 127 (1991) 354.
[2] R.G. Rizaev, E.A. Mamedov, V.P. Vislovskii, V.E. Sheinin, Appl. Catal. 83 (1992) 103.
[3] R. Nilsson, T. Lindblad, A. Andersson, Catal. Lett. 29 (1994) 409.
[4] A.T. Guttmann, R.K. Grasselli, J.F. Brazdil, US Patent US 4,746,641 (1988).
[5] Y. Moro-oka, W. Ueda, in: Catalysis, Vol. 11, Royal Chemical Society, Cambridge, UK, 1994, p. 223.
[6] H.W. Zanthoff, S. Buchholz, O.V. Ovsitser, Catal. Today 32 (1996) 291.
[7] J.F. Brazdil, A.M. Ebner, F.A.P. Cavalcanti, Appl. Catal. A 165 (1997) 51.
[8] Z. Hou, Q. Dai, X. Wu, G. Chen, Appl. Catal. A 161 (1997) 183.
[9] J.F. Brazdil, I.R. Little, J.B. Hazen, US Patent US 5,214,016 (1993).
[10] H.W. Zanthoff, S. Schaefer, G.-U. Wolf, Appl. Catal. A 164 (1997) 105.
[11] S. Albonetti, G. Blanchard, P. Burattin, F. Cavani, F. Trifiro, Eur. Pat. Appl. EP 691,306 A1 (1996).
[12] T. Birchall, A.W. Sleight, Inorg. Chem. 15 (1976) 868.
[13] F.J. Berry, M.E. Brett, W.R. Patterson, J. Chem. Soc., Dalton Trans. (1983) 9.
[14] F.J. Berry, M.E. Brett, J.G. Holden, A. Labarta, R. Rodriguez, J. Tejada, Inorg. Chim. Acta 105 (1985) 197.
[15] S. Hansen, K. Stahl, R. Nilsson, A. Andersson, J. Solid State Chem. 102 (1993) 340.
[16] R. Nilsson, T. Lindblad, A. Andersson, C. Song, S. Hansen, Stud. Surf. Sci. Catal. 82 (1994) 293.
[17] G. Centi, E. Foresti, F. Guarnieri, Stud. Surf. Sci. Catal. 82 (1994) 281.
[18] A. Andersson, S.L.T. Andersson, G. Centi, R.K. Grasselli, M. Sanati, F. Trifiro, Appl. Catal. A 113 (1994) 43.
[19] A. Landa-Cánovas, J. Nilsson, S. Hansen, K. Stahl, A. Andersson, J. Solid State Chem. 116 (1995) 369.
[20] G. Centi, P. Mazzoli, S. Peratoner, Appl. Catal. A 165 (1997) 273.
[21] R. Nilsson, T. Lindblad, A. Andersson, J. Catal. 148 (1994) 501.
[22] J. Nilsson, A. Landa-Cánovas, S. Hansen, A. Andersson, Catal. Today 33 (1997) 97.
[23] J. Nilsson, A. Landa-Cánovas, S. Hansen, A. Andersson, Stud. Surf. Sci. Catal. 110 (1997) 413.
[24] S. Albonetti, G. Blanchard, P. Burattin, T.J. Cassidy, S. Masetti, F. Trifiro, Catal. Lett. 45 (1997) 119.
[25] F.J. Berry, M.E. Brett, R.A. Marbrow, W.R. Patterson, J. Chem. Soc., Dalton Trans. (1984) 985.
[26] G. Centi, S. Perathoner, F. Trifiro, Appl. Catal. A: Gen. 157 (1997) 143.
[27] R. Catani, G. Centi, F. Trifiro, R.K. Grasselli, Ind. Eng. Chem. Res. 31 (1992) 107.
[28] G. Grosse, MOS-90, Version 2.2, Technical University of Munich, 1992.
[29] A. Brückner, H.W. Zanthoff, Colloids Surf. A: Physicochem. Eng. Aspects 158 (1999) 107.
[30] R. Haul, G. Dümbgen, Chem. -Ing. -Techn. 35 (1963) 586.
[31] N. Burriesci, F. Garbassi, M. Petrera, G. Petrini, J. Chem. Soc., Faraday Trans. 1 (78) (1982) 817.
[32] M.D. Allen, S. Poulston, E.G. Bithell, M. Goringe, M. Bowker, J. Catal. 163 (1996) 204.

[33] H.-G. Boyen, Macfit, Surface Analysis Software Package, Institute of Physics, University of Basle, Basle, Switzerland, 1996.
[34] J.H. Scofield, J. Electron Spectrosc. Relat. Phenom. 8 (1976) 129.
[35] M. Heber, W. Grünert, Top. Catal., in press.
[36] JCPDS-Powder Diffraction File, Joint Committee on Powder Diffraction Standards (JCPDS), 1601 Park Lane, Swarthmore, PA, USA.
[37] B. Darriet, J.O. Bovin, J. Galy, J. Solid State Chem. 19 (1976) 205.
[38] C. Rocchiccioli-Deltcheff, T. Dupruis, R. Franck, J. Chimie Phys. Biol. 67 (1970) 2037.
[39] G. Centi, S. Perathoner, Appl. Catal. A 124 (1995) 317.
[40] G. Centi, P. Mazzoli, Catal. Today 28 (1996) 351.
[41] G. Centi, F. Marchi, S. Perathoner, J. Chem. Soc., Faraday Trans. 92 (1996) 5151.
[42] G. Busca, A. Zecchina, et al., Catal. Today 20 (1994) 61.
[43] G. Busca, J.C. Lavalley, Spectrochim. Acta 42A (1986) 443.
[44] S.A. Buchholz, H.-W. Zanthoff, in: Proceedings of the DGMK-Symposium on Selective Oxidation in Petrochemistry, Hamburg, 8–9 October 1998, DGMK-Berichte 9803, 1998, p. 37
[45] F.J. Berry, M.E. Brett, Inorg. Chim. Acta 76 (1983) L205.
[46] G.J. Long, J.G. Stevens, L.H. Bowen, Inorg. Nucl. Chem. Lett. 51 (1969) 799.
[47] F.J. Berry, M.E. Brett, W.R. Patterson, J. Chem. Soc., Dalton Trans. (1983) 13.
[48] S. Poulston, N.J. Price, C. Weeks, M.D. Allen, P. Parlett, M. Steinberg, M. Bowker, J. Catal. 178 (1998) 658.
[49] D. Wagner, in: D. Briggs, M.P. Seah (Eds.), Practical Surface Analysis, 2nd Edition, Vol. 1, Chichester, 1990, Appendix 5.
[50] J. Mendialdua, R. Casanova, Y. Barbaux, J. Electron Spectrosc. Relat. Phenom. 71 (1995) 49.
[51] M. Heber, W. Grünert, J. Phys. Chem. B, in press.
[52] H. Poelman, L. Fiermans, Solid State Commun. 92 (1994) 669.
[53] A. Andersson, S.L.T. Andersson, G. Centi, R.K. Grasselli, M. Sanati, F. Trifiro, Stud. Surf. Sci. Catal. 75 (1993) 691.
[54] G. Grubert, W. Grünert, J. Rathouský, A. Zukal, G. Schulz-Ekloff, M. Wark, in: M.M.J. Treacy, B.K. Marcus, M.E. Bisher, J.B. Higgins (Eds.), Proceedings of the 12th International Zeolite Conference, Baltimore, USA, 5–10 July 1998, MRS Conference Proceedings, Vol. II, pp. 825–832.
[55] D. Wolf, M. Heber, W. Grünert, M. Muhler, J. Catal., submitted for publication.
[56] K. Hermann, M. Witko, R. Druzinic, A. Chakrabarti, B. Tepper, M. Elsner, A. Gorschlüter, H. Kuhlenbeck, H.-J. Freund, J. Electron Spectrosc. Relat. Phenom. 98/99 (1999) 245.
[57] M. Heber, W. Grünert, Materialwiss. Werkstofftechn., submitted for publication.
[58] E.P. Parry, J. Catal. 2 (1963) 371.
[59] K. Tanabe, Solid Acids and Bases — Their Catalytic Properties, Kodansha, Tokyo, and Academic Press, New York, 1970.
[60] H.W. Zanthoff, Habilitation thesis, Lehrstuhl für Technische. Chemie, Ruhr-University Bochum, Germany (1999).
[61] D.J. Stewart, O. Knop, C. Ayasse, F.W.D. Woodhams, Can. J. Chem. 50 (1972) 690.
[62] J. Nilsson, A. Landa-Cánovas, S. Hansen, A. Andersson, J. Catal. 160 (1996) 244.
[63] G. Fabbri, P. Baraldi, Anal. Chem. 44 (1972) 1325.
[64] G. Hausinger, H. Schmelz, H. Knözinger, Appl. Catal. 39 (1988) 267.
[65] Y. Nakagawa, T. Ono, H. Miyata, Y. Kubokawa, J. Chem. Soc., Faraday Trans. I 79 (1983) 2929.
[66] G. Centi, R.K. Grasselli, E. Patane, F. Trifiro, Stud. Surf. Sci. Catal. 55 (1990) 515.